JOURNAL OF Applied Polymer SCIENCE

Temperature Dependence of Fracture Behavior of PA6/OMMT Nanocomposites

A. Monami,[1] K. Reincke,[2] W. Grellmann,[2] B. Kretzschmar[3]

[1]Polymer Service GmbH Merseburg, Merseburg, Germany

[2]Center of Engineering Sciences, Materials Diagnostics/Materials Testing, Martin Luther University Halle-Wittenberg, Halle/Saale, Germany

[3]Leibniz Institute of Polymer Research e.V., Dresden, Germany

Correspondence to: A. Monami (E-mail: andrea.monami@psm.uni-halle.de)

ABSTRACT: The aim of this work was to characterize the fracture behavior of polyamide 6 (PA6) and PA6 reinforced with clay (organically modified montmorillonite) [PA6/OMMT] at different temperatures and under higher loading rate. Pure PA6 and PA6 with different amounts and two types of OMMT were investigated. The structure and morphology of the nanocomposites were analyzed by X-ray diffraction technique and transmission electron microscopy. The fracture behavior was evaluated using the instrumented Charpy impact test at different temperatures starting from −30 °C up to 50 °C. To determine the fracture toughness K_{Id} at higher temperatures, the equivalent-energy concept was used. Based on the *J*-value versus temperature diagrams, the brittle-to-tough transition temperature T_{BTT} of the materials was determined. It was found that the crack toughness as a function of temperature and the T_{BTT} are influenced by the content of OMMT and the morphology. There are indications that at low OMMT contents, the deformation behavior is dominated by the matrix properties. With increasing filler content, the influence of the nanostructure on T_{BTT} increases. The crack toughness of the nanocomposites with an intercalated morphology is higher than that of exfoliated ones, due to additional energy-dissipating mechanisms. © 2012 Wiley Periodicals, Inc. J. Appl. Polym. Sci 000: 000–000, 2012

KEYWORDS: fracture; toughness; nanocomposites; polyamides

Received 24 June 2011; accepted 14 July 2012; published online
DOI: 10.1002/app.38351

INTRODUCTION

Polymeric nanocomposites are interesting materials, since most of their mechanical properties can be improved by small amounts of filler. Therefore, the density of the nanocomposites is almost as low as of the matrix material that promises lightweight applications with good mechanical properties.

Polyamides (PA) reinforced with layered silicates, for example, montmorillonite (MMT) show good properties. MMT is often used as a reinforcing platelet-shaped mineral. The thickness of the platelets, each consisting of two tetrahedral sheets sandwiching one octahedral sheet,[1] is about 1 nm and the length can be about some 100 nm.[2,3] MMT can be organically modified, which is then referred to as organically modified montmorillonite (OMMT) and consists of the inorganic MMT and the chemical modification. The use of an organic modifier improves the compatibility of OMMT with the polymer and also helps to break up the OMMT powder during the preparation of the nanocomposites, because of the increased platelet distance.[4,5]

Besides completely unaffected clay, three different morphologies mainly occur in polymer/layered silicate nanocomposites: the exfoliated, the intercalated, and the hybrid structure. Usually, the aim is to get an exfoliated structure with an even and statistic distribution of the OMMT, which is assumed to show best mechanical properties.[6,7] Very often, the OMMT platelets are still intercalated and contain OMMT stacks. However, frequently, only a hybrid structure can be achieved in technical compounds.[6–9]

For OMMT/polymer materials, a great improvement of mechanical properties like strength and stiffness are often accompanied by a decrease in toughness[10] and crack toughness.[11] Toughness characterizes the total energy consumption capacity of a material, while crack toughness is directly related to the material's resistance against crack initiation. Crack toughness can be expressed by means of the fracture toughness *K* and the *J*-integral. Crack toughness is an important material property, since it limits the application fields of materials. It is very

sensitive to material's structure and morphology and therefore, the respective material parameters can be used for material development and optimization.

The properties of polymers are strongly influenced by the temperature, due to their viscoelastic nature. Therefore, it is important to study the influence of temperature on the properties of polymeric nanocomposites. There is still a lack of information about the influence of temperature on the fracture mechanics properties of polymeric nanocomposites, although the influence of temperature on the fracture mechanics properties of nonreinforced polymers has been studied extensively. There also exists some information about the temperature dependence of some mechanical properties of polymeric nanocomposites. But, the information of the correlation between temperature and fracture mechanics properties of nanocomposites is still missing, which will be investigated in this article.

The influence of temperature on the fracture mechanics properties of nonreinforced polyamide 6 (PA6) with and without impact modifier is well-known.[12,13] The resistance against unstable crack growth usually increases with rising test temperature. At lower temperatures, a plateau exists, where the materials behave brittle and crack toughness is nearly constant at a low level. At a critical temperature, the crack toughness of the polymers increases strongly and the material behavior changes from brittle to tough.[12,13] This brittle-to-tough transition temperature can be influenced by the used impact modifiers.[13] With a further increase of temperature, the crack propagation behavior changes at another critical temperature from an unstable to a stable manner.[12]

In contrast to fracture properties at different temperatures, the fracture properties of polymeric nanocomposites at room temperature, especially those based on a PA matrix with and without elastomeric modification, were investigated in some studies.[11,14–24] Very often, the concept of essential work of fracture (EWF) was applied,[14–19] but there are also studies to analyze the material's resistance against unstable crack propagation[11,20,21] and some research studies about the deformation behavior during tensile loading.[22–24]

Some of the studies described that the resistance of the materials against unstable crack initiation is reduced by the inhibition of the movement of the polymer molecules due to the OMMT platelets, and therefore the matrix deformation is limited.[18,20] Furthermore, it was mentioned that in intercalated nanocomposites, an additional deformation mechanism is possible: the OMMT stacks can break when hydrostatic tension is applied on them.[23] This can lead to the splitting, opening, or sliding of the stacks, depending on the orientation of the stacks with respect to the load direction.[23] These additional processes can dissipate energy what leads to a higher crack toughness of nanocomposites. Thus, the existence of some intercalated stacks in polymeric nanocomposites can be an interesting and simple way to increase the crack toughness.

All these already-mentioned studies about fracture properties were performed at room temperature. The dependence of mechanical properties on the temperature in polymeric nanocomposites is rarely investigated, even though the test temperature influences mechanical properties of polymeric materials due to their viscoelastic nature. Some studies were published, which report on the temperature behavior of polymeric nanocomposites. Thus, in Refs. 25–29 it was stated that with increasing temperature, the modulus of elasticity E_t and the tensile strength σ_M decrease while the area under the stress–strain diagram and the strain at break increase. Furthermore, fracture mechanics properties of PA6.6 nanocomposites as a function of temperature were investigated in Ref. 17. It was found that the materials' resistance against crack initiation, determined by the EWF approach, increases with increasing temperature until an optimum is reached. This optimum lies between 50 and 80 °C for PA6.6 and 80–100°C for PA6.6-nanocomposites reinforced with nanoparticles like TiO_2, SiO_2, or Al_2O_3.[17] There is still a lack of information about the temperature dependence of the fracture mechanics properties under impact loading, which represents a common kind of loading during application.

The aim of this work is, to investigate the influence of temperature on the fracture mechanics properties of PA6 and PA6/OMMT nanocomposites under impact loading and to determine the brittle-to-tough transition temperature T_{BTT}. Also, the influence of the different modification of OMMT on the fracture mechanics properties was determined. Additionally, structure and morphology were characterized by using X-ray diffraction (XRD) technique and transmission electron microscopy (TEM).

EXPERIMENTAL

Materials and Specimen Preparation

The investigated materials are based upon a PA6 matrix of the type Ultramid B27E01 supplied by BASF AG, Leuna, Germany. Reinforcement was accomplished using two different types of OMMT: Nanofil®5 and Nanofil®9 by Rockwood Clay Additives GmbH, Moosburg, Germany (formerly Süd-Chemie AG, Moosburg, Germany). These OMMTs have different chemical modifications[30] but the same density of MMT of 1.98 g/cm^3, which was used to calculate the MMT content in vol %[7] (for details, see Table I). The abbreviation "OMMT" denotes for MMT including the chemical modification, while the abbreviation "MMT" means only the inorganic part of the OMMT and is more useful for comparison of polymeric nanocomposites. The materials were conditioned at 70 °C and 68% humidity, until the mass was constant. The conditioned state matches the properties in application better.

Based on results of systematic in-house investigations of the influence of compounding conditions on the performance of PA6/OMMT nanocomposites, a one-step extrusion technology was used for the preparation. PA6 and OMMT were extruded in a corotating twin screw compounder ZE 25 UTS (Berstorff, Hannover, Germany) with $L/D = 36$, a temperature profile of 235–250 °C at 300 rpm, and a throughput of 10 kg/h to the final nanocomposite with the focused clay content. Afterward, multipurpose specimens of type 1A according to ISO 3167 were produced by injection-molding using Ergotech 100/420-310 (Demag, Germany).

Characterization

Structure and morphology influence the material properties strongly, and are therefore important to be investigated. For

Table I. Materials, Composition, and Additional Data

Material	OMMT content (wt %)	MMT content (wt %)	MMT content (vol %)	Chemical modification[30]	Recommended polymers[30]
PA6	0	0	0		
PA/N5-2	3	2	0.012	Distearyl-dimethyl-ammonium chloride	EVA, grafted PP, UP
PA/N5-6	9	6	0.035		
PA/N9-2	3	2	0.012	Stearylbenzyl-dimethyl-ammonium chloride	PBT, grafted PP, PA6, PA66
PA/N9-6	9	6	0.035		

nanocomposites, it is necessary to know the degree of exfoliation that can be analyzed by a combination of XRD technique and TEM.

To investigate the nanostructure, XRD measurements were performed in transmission mode with X-ray radiation (CuK_α) and measured with a Kratky camera by AntonPaar, Graz, Austria. These measurements can provide information about the presence of intercalated OMMT platelets and the distance between these parallelly arranged platelets.

To verify XRD results and to gain insight into the dispersion of the layered silicates within the polymeric matrix, a TEM investigation of ultrathin slices was performed using the transmission scanning microscope JEM 2010 by JEOL, Tokyo, Japan. The probes were taken out of the middle part of the specimens by cutting perpendicularly to the flow direction of the polymer melt. To get a rough value of the ratio of intercalated to exfoliated platelets, the number of exfoliated and the number of intercalated platelets, which can be seen on TEM images, were counted manually. The evaluated TEM images, one for each type of OMMT, were taken with a 50,000× magnification and contained 2 wt % MMT.

The fracture properties were characterized by using instrumented Charpy impact test (ICIT). The instrumentation of the Charpy impact test enables the registration of load–deflection (F–f) diagrams, which are the basis of the determination of the fracture parameters J_{Id}^{ST} and K_{Id}. These values are interpreted as the material's resistance against unstable crack initiation.[31]

For the ICITs, the shoulders of the multipurpose specimens were cut. The specimens were prismatic with length L = 80 mm, width W = 10 mm, and thickness B = 4 mm and they were notched with a razor blade. The notch depth a was 2 mm and support span s was 40 mm. The pendulum hammer speed for the examination of the nanocomposites was constant 1.5 m/s. The ICIT was performed at different test temperatures, starting from –30°C until reaching the highest temperature at which unstable crack growth occurs. All materials were tested at –30 °C, 0 °C, and at room temperature (23 °C). The selection of temperatures above room temperature depended on the highest temperature at which unstable crack growth occurs. The specimens were stored at the desired temperature in a temperature chamber for at least half an hour. Experience shows that this amount of time is enough for the temperature being equally distributed within specimens with the above-mentioned dimensions. The specimens were tested within a few seconds after removal from the temperature chamber.

Typical examples of F–f diagrams of notched specimens of the ICIT are shown in Figure 1. The type of diagrams reflects the deformation behavior of the materials, which can be linear-elastic [Figure 1(a)] or elastic–plastic [Figure 1(b)]. Based on the diagrams, the characteristic load value F_{gy} corresponding to the transition from linear-elastic to elastic–plastic behavior, the maximum load F_{max}, and the associated deflections f_{max} and f_{gy} were determined.

Using unnotched specimens for ICIT, the linear part of the resulting F–f diagrams of the unnotched specimens was analyzed and the dynamic flexural modulus E_d and the dynamic yield stress σ_d were determined using eqs. (1) and (2).

$$E_d = \frac{F_{gy} s^3}{4BW^3 f_{gy}} \tag{1}$$

$$\sigma_d = \frac{3F_{gy} s}{2BW^2} \tag{2}$$

The F–f diagrams, which were obtained by using notched specimens, were analyzed according to an in-house procedure.[31] The splitting of the energy consumed by the notched specimen into an elastic part A_{el} and a plastic part A_{pl} is possible, being the basis for the calculation of the J values J_{Id}^{ST} according to the evaluation method of Sumpter and Turner [eqs. (3)–(5)].[31]

$$J_{Id}^{ST} = \eta_{el} \frac{A_{el}}{B(W-a)} + \eta_{pl} \frac{A_{pl}}{B(W-a)} \frac{W - a_{eff}}{W-a} \tag{3}$$

with the effective crack length a_{eff}, Poisson's ratio ν, and the elastic part of the geometry function η_{el}

$$\eta_{el} = \frac{2F_{gy} s^2 (W-a)}{f_{gy} E_d BW^3} f^2\left(\frac{a}{W}\right)(1-\nu^2) \tag{4}$$

and the plastic part of the geometry function η_{pl}

$$\eta_{pl} = 2 - \frac{1 - \left(\frac{a}{W}\right)\left(0.892 - 4.476\frac{a}{W}\right)}{1.125 + 0.892\frac{a}{W} - 2.238\left(\frac{a}{W}\right)^2}. \tag{5}$$

Furthermore, fracture toughness K_{Id} was determined, according to eq. (6).

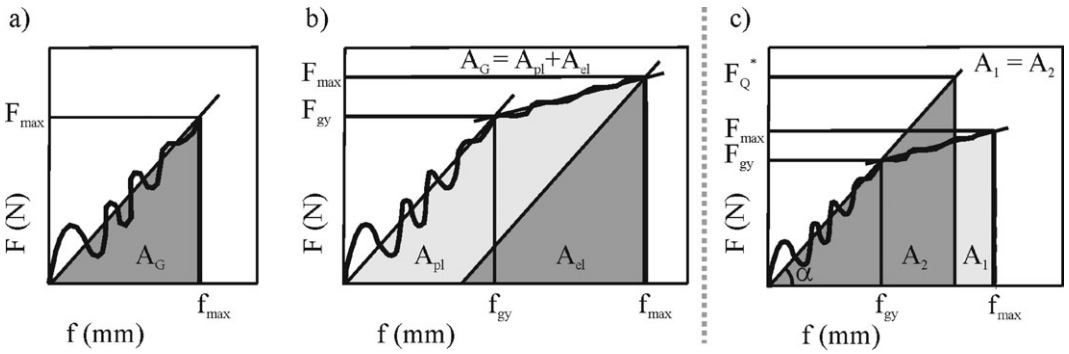

Figure 1. Schematic load–deflection (F–f) diagrams recorded during an instrumented Charpy impact test showing (a) linear-elastic behavior and (b) elastic–plastic deformation behavior; (c) analysis of a diagram showing elastic–plastic deformation behavior with the aim of determining the pseudo-elastic load F_Q^* during the application of the equivalent-energy concept.

$$K_{\mathrm{Id}} = \frac{F_{\max} s}{BW^{3/2}} f\left(\frac{a}{W}\right) \tag{6}$$

Requirement to determine the fracture toughness is an elastic material behavior with small scale yielding.[32] With increasing temperature, the material behavior changes to elastic–plastic deformation behavior and the determination of the fracture toughness is no longer reliable. To expand the range of the fracture toughness, the equivalent-energy concept was applied, where the fracture toughness $K_{\mathrm{Id}}{}^{\mathrm{E}}$ is determined instead of K_{Id} [see eqs. (7)–(9)]. The principle of the determination of the pseudo-elastic load F_Q^* is shown in Figure 1(c).

$$K_{\mathrm{Id}}^{E} = \frac{F_Q^* s}{BW^{3/2}} f\left(\frac{a}{W}\right) \tag{7}$$

with the pseudo-elastic load F_Q^* and the general deformation energy A_G

$$F_Q^* = \sqrt{2A_G \tan\alpha} \tag{8}$$

and the angle α

$$\tan\alpha = \frac{F_{\mathrm{gy}}}{f_{\mathrm{gy}}}. \tag{9}$$

Based on a dimensional analysis, the equivalent-energy concept can be used to determine the fracture toughness of ductile materials.[33] It is assumed that a single master curve exists that describes the nominal load versus load-line displacement curves of a specimen with analogous geometries, but different thicknesses. The area under this curve has a dimension of volumetric energy. Therefore, $F_{\max}$ can be substituted by the pseudo-elastic force F_Q^*.[33,34]

Using the determined fracture parameters, crack toughness–temperature (K_{Id}–T or $J_{\mathrm{Id}}{}^{\mathrm{ST}}$–$T$) diagrams were compiled and the brittle-to-tough transition temperature T_{BTT} was determined. The approach is shown in Figure 2. Two tangents are placed and their intersection is consistent with T_{BTT}.

Additionally to the fracture parameters, optical reflective microscopy was applied to investigate fracture toughness micromechanisms using digital microscope VHX 500F by Keyence to gain an overview and to determine the stable part of crack growth.

Micromechanical deformation mechanism were investigated using the scanning electron microscope (SEM) Ultra 55 plus by Zeiss. Therefore, the fracture surfaces of the specimens were sputtered with platinum Pt.

RESULTS AND DISCUSSION

Characterization of Morphology

The morphology of the nanocomposites was investigated with XRD technique and TEM. The results of XRD of the neat Nanofil 5, of the neat Nanofil 9, and of the nanocomposites are displayed in Figure 3. Pure Nanofil 5 and PA/N5-6 show two peak maxima. The peak at the higher reflexion angle corresponds to a higher harmonic oscillation.[35] Hence, the platelet distance is derived from the smaller reflexion angle. In PA/N5-6, clearly detectable stacks exist and the material's structure is intercalated. The platelet distance equates to 4 nm, being slightly higher than the distance of 3 nm in the neat OMMT powder. PA/N5-2 has a small peak corresponding to a platelet distance of 7.7 nm. Thus, all nanocomposites containing Nanofil 5 have an intercalated morphology. The intercalated

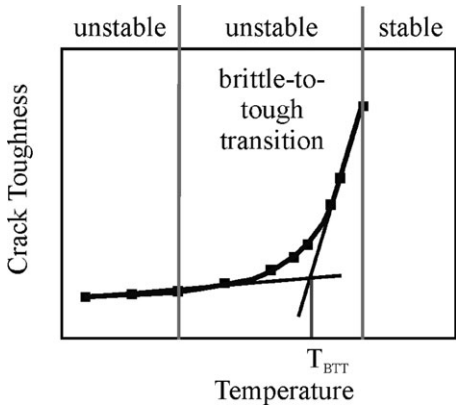

Figure 2. Principle of the determination of the brittle-to-tough transition temperature T_{BTT} from results of the ICIT as a function of the test temperature.

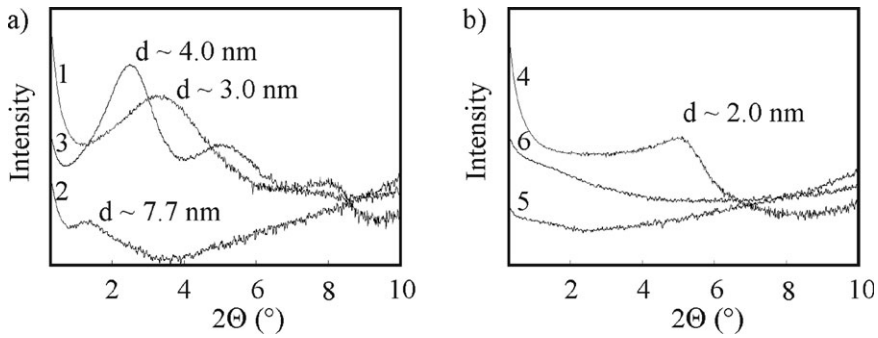

Figure 3. XRD plot of (a) pure Nanofil®5 (1), PA/N5-2 (2), and PA/N5-6 (3), and of (b) pure Nanofil®9 (4), PA/N9-2 (5), and PA/N9-6 (6).

morphology was expected, because the side groups of the alkylammonium chloride, which is used as the chemical modification of Nanofil 5, is more compatible with polyolefines than with PA (see also Table I). Therefore, the compatibility between Nanofil 5 and PA6 is lower than between Nanofil 9 and PA6, leading to an intercalated morphology of PA/N5. On the contrary, PA/N9 is in the exfoliated state, independently of the OMMT content, since there are no peaks in the XRD plots.

The exemplary TEM images in Figure 4 confirm the results of the XRD measurements. PA/N5-2 shows not only a lower degree of orientation of the platelets but also a typical hybrid structure consisting of single exfoliated platelets and some stacks of intercalated OMMT. A rough quantitative analysis showed that around a quarter of the platelets are organized within stacks. PA/N9-2 is well exfoliated and has orientated platelets. The orientation is due to the injection-molding of the specimen. These results are also confirmed by the TEM images of PA/N5-6 and PA/N9-6. These images additionally show the higher number of platelets within the matrix due to the increase of MMT-content.

Characterization of Mechanical Properties

The dynamic flexural modulus E_d and the dynamic yield stress σ_d of PA/N5-2, PA/N5-6, PA/N9-2, and PA/N9-6 at different temperatures are shown in Figure 5. The stiffness, expressed by the dynamic flexural modulus E_d, decreases steadily with rising temperature. This behavior is independent of the filler content, but the value of E_d at a given temperature rises with increasing

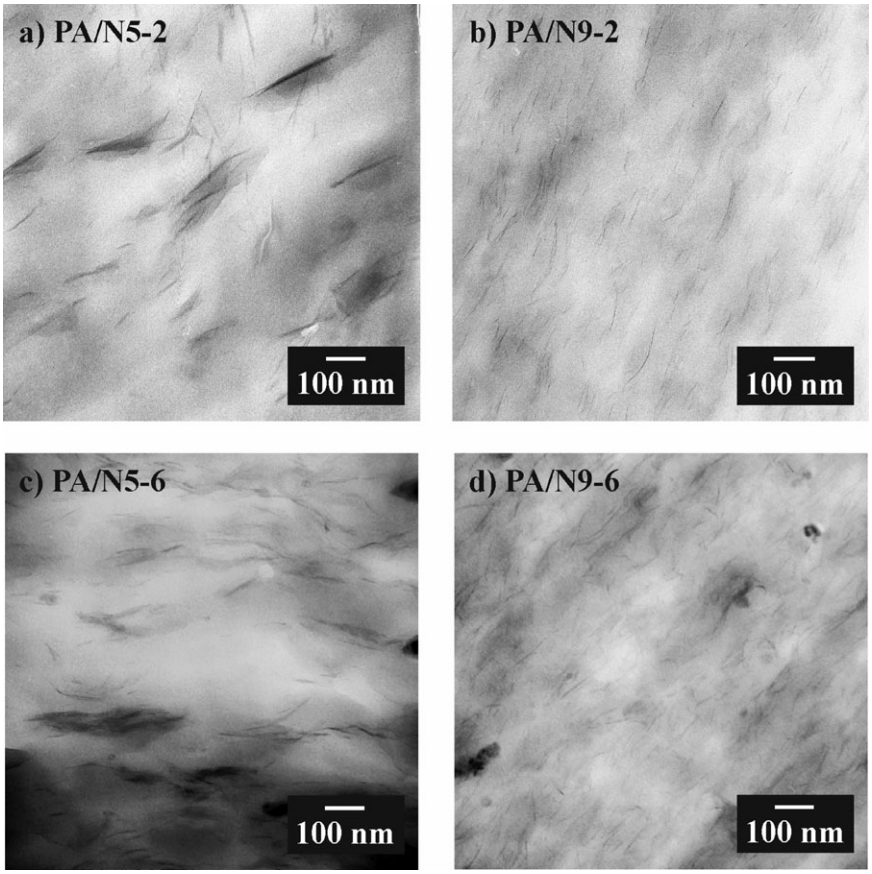

Figure 4. Examples of TEM images of (a) PA/N5-2, (b) PA/N9-2, (c) PA/N5-6, and (d) PA/N9-6.

Applied Polymer SCIENCE

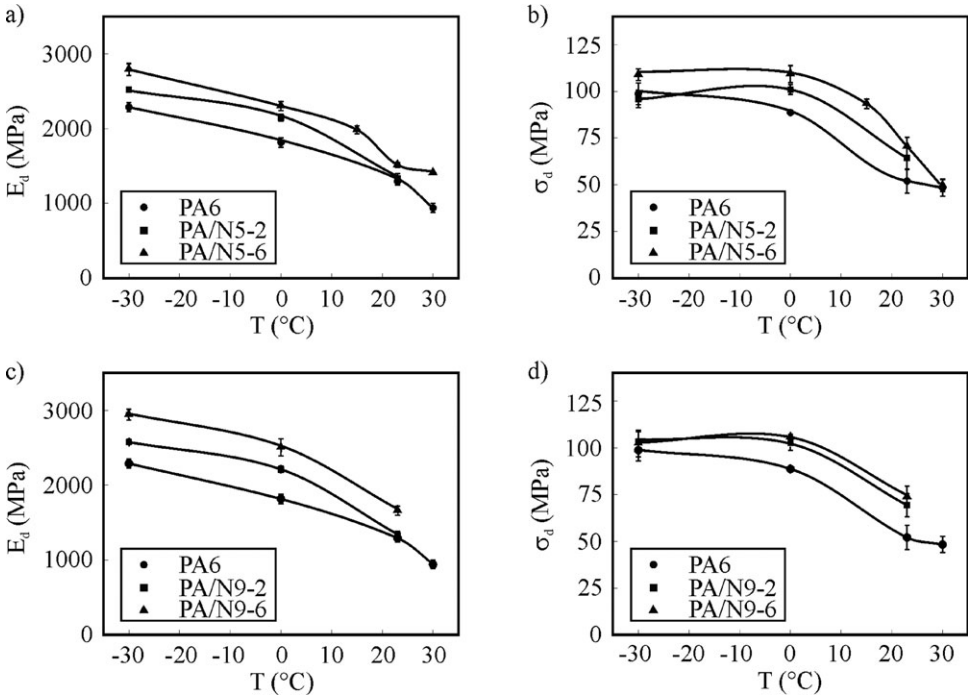

Figure 5. Dynamic flexural modulus E_d and dynamic yield stress σ_d of PA/N5 (a) and (b) and PA/N9 (c) and (d) with increasing MMT content at different testing temperatures.

MMT content. The dynamic yield stress σ_d of the nanocomposites stays nearly constant until 0°C and decreases then strongly. In contrast, the dynamic yield stress of neat PA6 is already reduced at 0 °C. The influence of the temperature on the dynamic flexural modulus and the dynamic yield stress, which are a measure of stiffness and strength, is therefore different that is based on the structure of the material. The decrease of strength and stiffness is in good agreement with literature.[29,34] Concluding, it can be stated that the OMMT enhances the strength of the materials at lower temperatures compared to the neat matrix, except for PA/N5-2 at −30 °C. The higher the amount of MMT, the higher is the strength. This is in agreement with the expected increase of strength and stiffness in nanocomposites due to a higher amount of MMT. In this study, strength and stiffness are not influenced by the state of exfoliation, since the E_d and σ_d values for PA/N5 and PA/N9 are comparable.

Characterization of Fracture Mechanics Properties

The fracture mechanics properties were characterized using the ICIT. Examples of *F–f* diagrams from ICIT of PA/N5-2 and PA/N9-2 at selected test temperatures are presented in Figure 6. At low temperatures, linear-elastic material behavior dominates. With increasing temperature, the maximum force F_{max} and the deformation at maximum force f_{max} increase. The material behavior changes from linear-elastic to elastic–plastic behavior with increasing temperature. This transition appears for the nanocomposites between 23 and 40 °C. With a further rise of the temperature, the stable crack growth dominates. Therefore, the material's resistance against unstable crack growth can no longer be determined. At low temperatures and at room temperature, PA/N5-2 and PA/N9-2 show quite similar *F–f* diagrams with similar material behavior. At 40 °C, the difference between the behavior of PA/N5-2 and PA/N9-2 is obvious. The maximum force F_{max} and the deformation at maximum force

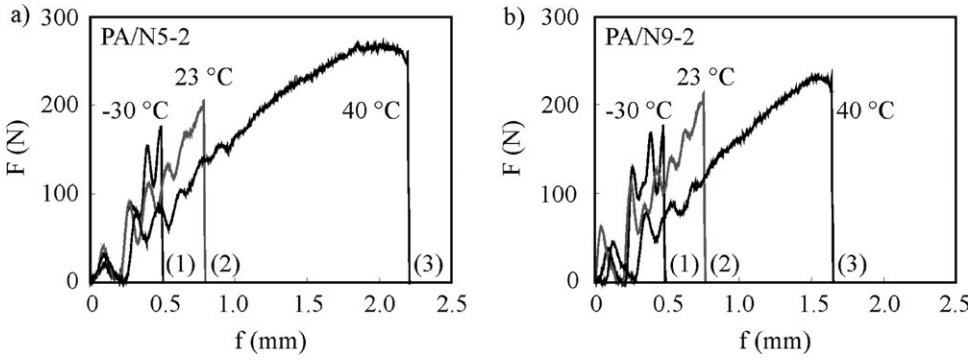

Figure 6. Selected load–deflection (*F–f*) diagrams of PA/N5-2 (a) and PA/N9-2 (b) at different testing temperatures.

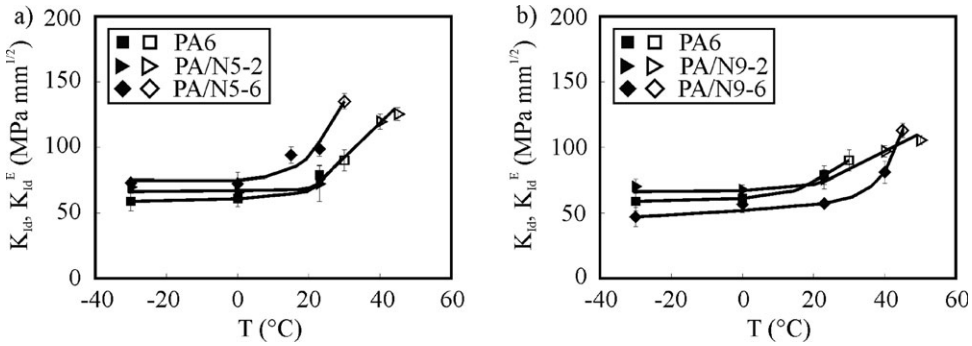

Figure 7. Fracture toughness K_{Id} (full symbols) and K_{Id}^E (open symbols) of PA/N5 (a) and PA/N9 (b) at varying test temperatures.

f_{max} are higher, which is connected to more pronounced energy consumption.

Characterization of the Influence of Temperature on Properties

The ICIT was performed at different temperatures. The resulting fracture toughness values as a function of temperature are shown in Figure 7. To distinguish K_{Id} and $K_{Id}^{E,}$ values of K_{Id}^E are marked by open symbols. The temperature dependence of the fracture toughness of pure PA6, PA/N5-2, and PA/N9-2 is quite similar. In nanocomposites with 6 wt % MMT, the influence of the type of OMMT on the fracture toughness as a function of temperature is more pronounced. The fracture toughness of PA/N5-6 increases strongly while the fracture toughness of PA/N9-6 decreases with rising temperature, compared to the matrix values. PA/N9-6 is in the exfoliated state, as discussed above on the basis of XRD and TEM results. This structure results in a higher number of single platelets within the matrix. Therefore, a higher load-bearing capacity of the exfoliated PA/N9 was expected with respect to PA/N5, due to its intercalated structure.

In Figure 8, the J values are shown as a function of the test temperature, comparing the different materials with the same MMT content within one chart. Similarly to the fracture toughness $K_{Id,}$ J values increase with rising temperature, due to the increasing matrix mobility. This facilitates energy-consuming deformation processes, leading to an increase in the energy-determined J values at higher temperatures. At temperatures higher than ~10 °C, the influence of the OMMT type becomes larger. The J values of PA/N5-2 and PA/N5-6 are higher than the J values of PA/N9-2 and PA/N9-6 at comparable temperatures. This result may be explained by the existence of energy-consuming deformations like opening, sliding, or splitting of the stacks that are only possible within the OMMT stacks of the intercalated PA/N5.[21,23]

Energy-consuming micromechanical deformations that occur during loading are indicated on the fracture surfaces, for example, by whitening or the occurrence of voids and fibrils. The size of the areas with plastic deformation changes depending on the temperature. This is schematically illustrated in Figure 9 and complemented with some selected light-microscopic images. With increasing temperature, the size of the damage area grows. At room temperature, a small area of stable crack propagation can be detected that increases with rising temperature. This is optically characterized by a white smooth crack surface. At a specific temperature, 50 °C in this study, stable crack growth becomes dominant.

SEM images (see Figure 10) show typical evidence of micromechanical deformations on the fracture surface of PA6 and nanocomposites containing 2 wt % Nanofil 5 or Nanofil 9, which were tested at different increased temperatures. At a testing temperature of 30 °C, the surface of specimens of PA6 is quite smooth between single ramps with earing. The surfaces of the nanocomposites show typical fracture parabola, combined with holes and filaments, which are typical signs of micromechanical plastic deformations of polymers.

Determination of the Brittle-to-Tough Transition Temperature T_{BTT}

As mentioned above, one aim of the investigations was the determination of the brittle-to-tough transition temperature.

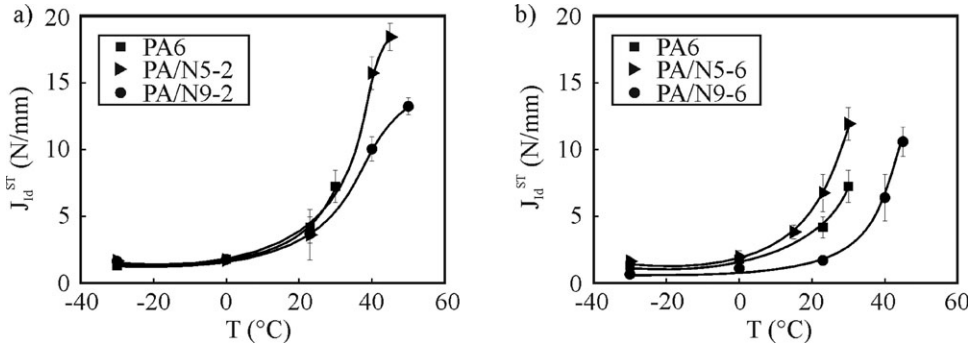

Figure 8. J values J_{Id}^{ST} at different temperatures of PA6, PA/N5-2, and PA/N9-2 (a) and PA6, PA/N5-6, and PA/N9-6 (b).

Applied Polymer SCIENCE

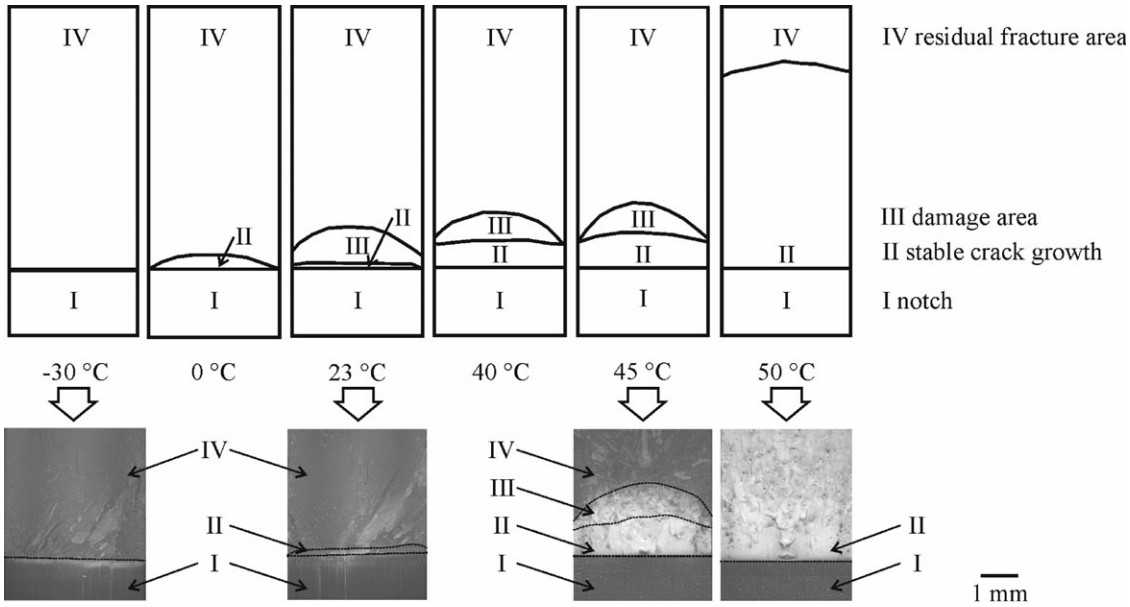

Figure 9. Schematic diagram of fracture surfaces of nanocomposites tested at different temperatures and accordant optical micrographs of PA/N5-2.

Within the investigated temperature range, the brittle-to-tough transition of the materials occurs. The application of the equivalent-energy concept to determine K_{Id}^{E} makes it possible to obtain fracture toughness values also at higher temperatures. Hence, the brittle-to-tough transition temperature T_{BTT} can be determined based on the fracture toughness–temperature diagrams and on the J value–temperature diagrams (Table II). The results of T_{BTT} based on the fracture toughness and the results based on J values differ. Mostly, the difference is small, except for PA6 and PA/N5-6.

Principally, it is possible to determine T_{BTT} using either K_{Id} and K_{Id}^{E} or J_{Id}^{ST} as a function of temperature, but with increasing temperature, the increase in the J values is higher than the increase in fracture toughness,[34] compared to their corresponding values at lower temperatures (see Figures 7 and 8). Therefore, it can be assumed that the materials' resistance against unstable crack initiation as a function of temperature is controlled by the energy uptake. That means, that the materials' resistance against unstable crack initiation is neither dominantly determined by the part of the strength nor by the part of the deformation. Additionally, the placement of the tangent at higher temperatures is easier for J_{Id}^{ST}–T diagrams and the results are therefore more reliable. Because of these reasons, T_{BTT} should be determined in this case from the J_{Id}^{ST}–temperature plots. The following discussion is therefore only related to T_{BTT} based on J values.

The brittle-to-tough transition temperature T_{BTT} of the materials is close to room temperature, except for PA/N9-6, where T_{BTT} is 35 °C. Therefore, one can expect a quite brittle material behavior of PA/N9-6 at room temperature. In materials with 2 wt % MMT, the matrix dominates the temperature-dependent deformation behavior, but in nanocomposites with 6 wt % MMT, the influence of the platelets increases. The T_{BTT} is influenced by the morphology of the materials. As mentioned above, PA/N9-6 has an exfoliated structure. Therefore, the OMMT platelets reduce the ability of the polymer matrix to consume energy by plastic deformation. Hence, crack toughness decreases and T_{BTT} increases. PA/N5-6 has a strongly intercalated structure that enables energy-consuming plastic deformation of the matrix, as shown by light microscopic images. Additionally, energy-consuming deformation of the OMMT stacks itself are possible[21,23] what increases the crack toughness and keeps the T_{BTT} constant, compared to the matrix value. This result is in accordance to the literature results,[21,23] which were determined

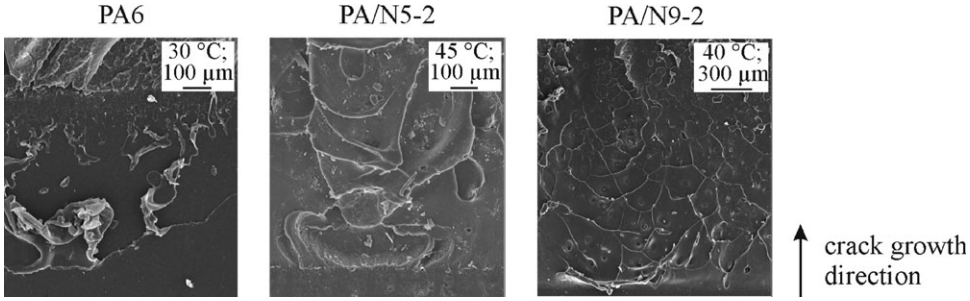

Figure 10. Selected SEM images of the fracture surfaces of PA6 (tested at 30 °C), PA/N5-2 (45 °C), and PA/N9-2 (40 °C).

Table II. Brittle-to-Tough Transition Temperatures T_{BTT}, Derived from Different Fracture Mechanics Parameters

	T_{BTT} (°C)	
Materials	T_{BTT}^{K} [a]	T_{BTT}^{J} [b]
PA6	14	19
PA/N5-2	27	21
PA/N5-6	19	17
PA/N9-2	18	19
PA/N9-6	38	35

[a]Derived from K_{Id}–T diagrams, [b]Derived from J_{Id}^{ST}–T diagrams.

at room temperature. With increasing MMT content and temperature, the energy-consuming deformation of the stacks can gain influence on the materials' resistance against unstable crack initiation.

CONCLUSIONS

Neat PA6 and PA6 nanocomposites containing 2 and 6 wt % inorganic MMT were analyzed. The MMT was modified with two different modifiers, so that two types of OMMT resulted: Nanofil 5 and Nanofil 9. The morphology of the materials was characterized by XRD measurements and TEM, which showed that PA/N5 is in the intercalated state and PA/N9 is exfoliated, independently of the MMT content.

The dynamic flexural modulus E_d, the dynamic yield stress σ_d, and the fracture mechanics parameters fracture toughness K_{Id} and the J value J_{Id}^{ST} were determined under impact-like loading conditions as a function of temperature. To determine the fracture toughness values also at higher temperatures, the equivalent-energy concept was applied and K_{Id}^{E} was determined.

With increasing temperature, the dynamic flexural modulus and the dynamic yield stress decrease, while the fracture toughness and the J values increase. Both fracture mechanics parameters are influenced by the MMT content and the type of modifier. The influence of the type of modification increases with increasing MMT content. Using 2 wt % MMT, especially the fracture toughness is only little influenced by the type of the modifier. When using 6 wt % MMT, the modifier and the degree of exfoliation determine the fracture mechanics parameters. In comparison to the matrix values and at comparable temperatures, fracture mechanics values are smaller, if the material is exfoliated and larger, if the material is intercalated. That leads to a clearly higher T_{BTT} for PA/N9-6, while T_{BTT} of PA/N5-6 remains almost at the level of matrix value. So, an intercalated structure has the advantage of a lower brittle-to-tough transition temperature.

It can be concluded that PA6 can be reinforced with OMMT, without increasing the brittle-to-tough transition temperature T_{BTT}. This property depends on the MMT content and the degree of exfoliation. At low MMT contents, the deformation behavior of the matrix dominates. With increasing MMT content, an exfoliated structure leads to an increase in T_{BTT}, but an intercalated one results in almost constant T_{BTT}.

ACKNOWLEDGMENTS

The authors thank the German federal state of Saxony-Anhalt for the financial support within the framework of the Cluster of Excellence "Nanostructured Materials", for the subproject NC1 "Influence of the exfoliation on the mechanical and fracture mechanics properties of polymeric nanocomposites". Special thanks go to A. Pießold, a former student of Prof. W. Grellmann (Martin Luther University Halle-Wittenberg, Germany), to S. Goerlitz, (Martin Luther University Halle-Wittenberg, Institute of Physics, Germany), and to R. Boldt (IPF Dresden, Germany).

REFERENCES

1. Murray, H. H. Kirk-Othmer Encyclopedia of Chemical Technology; Wiley, New York **2000.**
2. Wu, Z.; Zhou, C.; Zhu, N. *Polym. Test.* **2002,** *21*, 479.
3. Kojima, Y.; Usuki, A.; Kawasumi, M.; Okada, A.; Fukushima, Y.; Kurauchi, T.; Kamigaito, O. *J. Mater. Res.* **1993,** *8*, 1185.
4. Sharma, S. K.; Nayak, S. K. *Polym. Degrad. Stab.* **2009,** *94*, 132.
5. Akkapeddi, M. K. *Polym. Compos.* **2000,** *21*, 576.
6. Dennis, H. R.; Hunter, D. L.; Chang, D.; Kim, S.; White, J. L.; Cho, J. W.; Paul, D. R. *Polymer* **2001,** *42*, 9513.
7. Aït Hocine, N.; Médéric, P.; Aubry, T. *Polym. Test.* **2008,** *27*, 330.
8. Liu, T. X.; Liu, Z. H.; Ma, K. X.; Shen, L.; Zeng, K. Y.; He, C. B. *Compos. Sci. Technol.* **2003,** *63*, 331.
9. Tjong, S. C.; Bao, S. P. *J. Polym. Sci. B Polym. Phys.* **2004,** *42*, 2878.
10. Hasegawa, N.; Okamoto, H.; Kato, M.; Usuki, A.; Sato, N. *Polymer* **2003,** *44*, 2933.
11. Kelnar, I.; Scudla, J.; Kotek, J.; Kretzschmar, B.; Leuteritz, A. *Polym. Test.* **2006,** *25*, 697.
12. Langer, B.; Seidler, S.; Grellman, W. In Deformation and Fracture Behaviour of Polymers; Grellman, W., Seidler, S., Eds.; Springer: Berlin, Heidelberg, New York, **2001,** p 209.
13. Bethge, I.; Reincke, K.; Seidler, S.; Grellman, W. In Deformation and Fracture Behaviour of Polymers; Grellman, W., Seidler, S., Eds.; Springer: Berlin, Heidelberg, New York, **2001,** p 243.
14. Qiao, Y.; Avlar, S.; Chakravarthula, S. S. *J. Appl. Polym. Sci.* **2005,** *95*, 815.
15. Avlar, S.; Qiao, Y. *Compos. Appl. Sci. Manuf.* **2005,** *36*, 624.
16. Vu, H. N.; Vermogen, A.; Gauthier, C.; Masenelli-Varlot, K.; Cavaillé, J. Y. *J. Polym. Sci. B Polym. Phys.* **2008,** *46*, 1820.
17. Zhang, H.; Zhang, Z.; Yang, J.-L.; Friedrich, K. *Polymer* **2006,** *47*, 679.
18. Lim, S. H.; Dasari, A.; Wang, G. T.; Yu, Z. Z.; Mai, Y. W.; Yuan, Q.; Liu, S.; Yong, M. S. *Compos. B Eng.* **2010,** *41*, 67.
19. Tjong, S. C.; Bao, S. P. *J. Polym. Sci. B Polym. Phys.* **2005,** *43*, 585.
20. Lim, S. H.; Dasari, A.; Yu, Z. Z.; Mai, Y. W.; Liu, S.; Yong, M. S. *Compos. Sci. Technol.* **2007,** *67*, 2914.

21. Kelnar, I.; Kotek, J.; Kaprálková, L.; Munteanu, B. S. *J. Appl. Polym. Sci.* **2005,** *96*, 288.

22. Na, B.; Xu, W.; Lv, R.; Tian, N.; Li, Z.; Su, R.; Fu, Q. *J. Polym. Sci. B Polym. Phys.* **2010,** *48*, 514.

23. Kim, G. M.; Lee, D. H.; Hoffmann, B.; Kressler, J.; Stöppelmann, G. *Polymer* **2001,** *42*, 1095.

24. Kim, G. M.; Goerlitz, S.; Michler, G. H. *J. Appl. Polym. Sci.* **2007,** *105*, 38.

25. Bao, S. P.; Tjong, S. C. *Mater. Sci. Eng. A* **2008,** *485*, 508.

26. Mallick, P. K.; Zhou, Y. *J. Mater. Sci.* **2003,** *38*, 3183.

27. Shah, D.; Maiti, P.; Jiang, D. D.; Batt, C. A.; Giannelis, E. P. *Adv. Mater.* **2005,** *17*, 525.

28. van Rijswijk, K.; Lindstedt, S.; Vlasveld, D. P. N.; Bersee, H. E. N.; Beukers, A. *Polym. Test.* **2006,** *25*, 873.

29. Vlasveld, D. P. N.; Vaidya, S. G.; Bersee, H. E. N.; Picken, S. J. *Polymer* **2005,** *46*, 3452.

30. Süd-Chemie. Nanofil: Active NanoFillers for Polymer Applications, Süd-Chemie AG **2003.**

31. Grellmann, W.; Seidler, S.; Hesse, W. MPK-ICIT, Testing of Plastics-Instrumented Charpy Impact Test; Procedure for Determining the Crack Resistance Behaviour Using the Instrumented Charpy Impact Test, Part 1: Determination of Characteristic Fracture Mechanics Parameters for Resistance Against Unstable Crack Propagation, **2012.** Available at http://www2.iw.uni-halle.de/ww/mpk/p_e.pdf.

32. Grellmann, W. In Deformation and Fracture Behaviour of Polymers; Grellman, W., Seidler, S., Eds.; Springer-Verlag: Berlin, Heidelberg, New York, **2001,** p 3.

33. Witt, F. J.; Mager, T. R. *Nucl. Eng. Des.* **1971,** *17*, 91.

34. Grellmann, W.; Che, M. *J. Appl. Polym. Sci.* **1997,** *66*, 1237.

35. Ton-That, M. T.; Leelapornpisit, W.; Utracki, L.; Perrin-Sarazin, F.; Denault, J.; Cole, K.; Bureau, M. *Polym. Eng. Sci.* **2006,** *46*, 1085.